Synergy of phosphate recovery from sludge-incinerated ash and coagulant production by desalinated brine

Wang, Xiangyang; Shi, Chen; Hao, Xiaodi; van Loosdrecht, Mark C.M.; Wu, Yuanyuan

DOI
10.1016/j.watres.2023.119658

Publication date
2023

Document Version
Final published version

Published in
Water Research

Citation (APA)
Wang, X., Shi, C., Hao, X., van Loosdrecht, M. C. M., & Wu, Y. (2023). Synergy of phosphate recovery from sludge-incinerated ash and coagulant production by desalinated brine. *Water Research*, *231*, Article 119658. https://doi.org/10.1016/j.watres.2023.119658

Water Research 231 (2023) 119658

Contents lists available at ScienceDirect

Water Research

journal homepage: www.elsevier.com/locate/watres

Synergy of phosphate recovery from sludge-incinerated ash and coagulant production by desalinated brine

Xiangyang Wang [a], Chen Shi [a], Xiaodi Hao [a,*], Mark C.M. van Loosdrecht [a,b], Yuanyuan Wu [a]

[a] Sino-Dutch R&D Centre for Future Wastewater Treatment Technologies/Key Laboratory of Urban Stormwater System and Water Environment, Beijing University of Civil Engineering & Architecture, Beijing 100044, China
[b] Dept. of Biotechnology, Delft University of Technology, van der Maasweg 9, 2629 HZ Delft, the Netherlands

ARTICLE INFO

Keywords:
Waste activated sludge (WAS)
Incineration
Ash
Phosphorus recovery
Metals' recovery
Coagulants

ABSTRACT

Wet-chemical approach is widely applied for phosphate recovery from incinerated ash of waste activated sludge (WAS), along with metals removed/recovered. The high contents of both aluminum (Al) and iron (Fe) in WAS-incinerated ash should be suitable for producing coagulants with some waste anions like Cl^- and SO_4^{2-}. With acid (HCl) leaching and metals' removing, approximately 88 wt% of phosphorus (P) in the ash could be recovered as hydroxylapatite (HAP: $Ca_5(PO_4)_3OH$); Fe^{3+} in the acidic leachate could be selectively removed/recovered by extraction with an organic solvent of tributyl phosphate (TBP), and thus a $FeCl_3$-based coagulant could be synthesized by stripping the raffinate with the original brine (containing abundant Cl^- and SO_4^{2-}). Furthermore, a liquid poly-aluminum chloride (PAC)-based coagulant could also be synthesized with Al^{3+} removed from the ash and the brine, which behaved almost the same in the coagulation performance as a commercial coagulant on both phosphate and turbidity removals. Both P-recovery from the ash and coagulant production associated with the brine would enlarge the markets of both 'blue' phosphate and 'green' coagulants.

1. Introduction

The emerging phosphorus (P) crisis calls for efficient and sustainable P-recovery from wastes/wastewater. It has been practiced to recover phosphorus from wastewater and/or waste activated sludge (WAS) (Jupp et al., 2021; Liu et al., 2021; Ma and Rosen, 2021), ranging from struvite (Hao et al., 2013) to vivianite (Hao et al., 2022b; Wijdeveld et al., 2022). However, the proper environments suitable for formation of both struvite and vivianite are relatively strict (Hao et al., 2022b, 2013; Prot et al., 2021), and moreover P-recovery efficiencies of struvite and vivianite are not very high, at 15–30% and 40–70%, respectively (Chrispim et al., 2019; van der Kooij et al., 2020; Wijdeveld et al., 2022; Wilfert et al., 2015). In another approach to P-recovery, WAS-incinerated ash (5–10 P% or 11–23 P_2O_5%) have a high potential in the P-recovery efficiency, up to 90% (Fang et al., 2020; Jupp et al., 2021; Liu et al., 2021). Furthermore, incineration has been identified as an ultimate approach to disposing WAS (Galey et al., 2022; Hao et al., 2020a; Ma and Rosen, 2021). As a result, P-recovery from WAS-incinerated ash would become a mainstream approach to handling WAS, especially under the current condition that European counties generally emphasize to cover at 80% influent P-load from wastewater treatment (Jupp et al., 2021; Liu and Qu, 2016).

In practice, P-recovery techniques from WAS-incinerated ash have become relatively mature. Among others, wet-chemical approaches seem the most sustainable methods (Fahimi et al., 2021), followed by thermochemical methods (Fang et al., 2020; Galey et al., 2022; Liu et al., 2021). However, each of these techniques involves metal-removing processes. Indeed, WAS-incinerated ash contains both heavy metals (copper/Cu, zinc/Zn, lead/Pb, chromium/Cr, cadmium/Cd, mercury/Hg and nickel/Ni) and ordinary metals (calcium/Ca, magnesium/Mg, aluminum/Al, iron/Fe, sodium/Na and potassium/K) (Boniardi et al., 2021; Geng et al., 2020). Particularly, the contents of Al and Fe are so high as 6–18.8% and 2.4–14.5% (wt), respectively (Liang et al., 2019; Petzet et al., 2012; Smol et al., 2020), which could be utilized to produce coagulants/flocculants in wastewater treatment. Thus, recycling Al and Fe seems necessary associated with P-recovery towards a circular/blue economy (Hao et al., 2022a).

There are some limited studies on reusing Al as a precipitant (Morf et al., 2019; Petzet et al., 2012, 2011), and clearly some in-depth researches need to be carried out, especially for reusing Fe (Cohen and Enfält, 2018). Different from Al, Fe cannot be extracted by alkaline dissolution, but it can be extracted by some organic solvents, including

* Corresponding author.
E-mail address: haoxiaodi@bucea.edu.cn (X. Hao).

https://doi.org/10.1016/j.watres.2023.119658
Received 8 November 2022; Received in revised form 17 January 2023; Accepted 22 January 2023
Available online 23 January 2023

tributyl phosphate (TBP) (Wei et al., 2016; Yi et al., 2020), methyl isobutyl ketone (MIBK) (Saji and Reddy, 2001), di-(2-ethylhexyl)phosphoric acid (D2EHPA) (Azizitorghabeh et al., 2016), primary amine N1923 (Deep et al., 2007), etc. Potential reuse of Al and Fe should orient towards producing coagulants/flocculants. Under the circumstance, available anions like Cl^- and SO_4^{2-} would play an important role in reusing Al and Fe.

On the other hand, seawater desalination (SWD) has become a trend of acquiring freshwater along/near coastal areas (Jones et al., 2019; Pistocchi et al., 2020). The brine from desalination contains a high salt concentration, containing such anions as Cl^- and SO_4^{2-}, up to 41,829 and 6050 mg/L, respectively (Ortiz-Albo et al., 2019). Both Cl^- and SO_4^{2-} can be extracted from the brine by some methods, including adsorption (Qi et al., 2020), nanofiltration (NF) (Pérez-González et al., 2015) and electrodialysis (ED) (Zhang et al., 2009). Thus, the Cl^- and SO_4^{2-}-rich brine could have a considerable potential in producing coagulants/-flocculants with Al^{3+} and Fe^{3+} from WAS-incinerated ash, which has been preliminarily testified in our recent work (Hao et al., 2022a). In principles, a small stock of cations or anions should be transported to a large stock of anions or cations for producing coagulants/flocculants, like aluminum chloride/$AlCl_3$, ferric chloride/$FeCl_3$, poly-aluminum chloride/PAC (Hao et al., 2022a), poly ferric chloride/PFC, poly ferric sulfate/SPFS, poly aluminum ferric chloride/PAFC, and polymeric aluminum ferric sulfate/PAFS.

With this study, phosphate from WAS-incinerated ash was recovered as a main product, and both Fe and Al were removed to purify phosphate and then utilized to produce two coagulants as by-products, as shown in Fig. 1. There were three steps in the study: i) to remove Fe^{3+} and produce $FeCl_3$-based coagulant with the brine; ii) to recover phosphate in the form of Ca-P; iii) to remove Al^{3+} and produce PAC coagulant with the brine.

2. Materials and methods

2.1. Sources of WAS-incinerated ash and desalinated brine

WAS-incinerated ash was prepared by incinerating actual WAS from a WWTP in Beijing for 6 h in a lab-scale muffle furnace (850 °C), followed by drying at 105 °C for 12 h. Then, WAS-incinerated ash was naturally cooled down in the furnace and ground in a mortar, down to < 500 μm in particle size. Desalinated brine was prepared by evaporating seawater, with 50% water content evaporated.

Acid leaching of WAS-incinerated ash was carried out in a batch mode with magnetic stirrers on the bottoms of beakers (500 ml) at room temperature. Then, mixed liquor (leachate) in beakers was separated by 0.22 μm-filter membrane to determine the concentrations of P and metals like Al^{3+}, Fe^{3+}, Ca^{2+}, Mg^{2+}, etc.

2.2. Phosphate recovery as a Ca-P product

After extracting Fe^{3+}, the raffinate were adjusted with 1.0 mol/L NaOH up to pH = 3–4 to separate heavy metals-poor phosphate in the form of Al-P (an intermediate). When Al-P was dissolved again in an alkaline solution (up to pH = 13), a part of high valent metals was generally insoluble in the alkaline solution (Petzet et al., 2012). As a result, dissolved PO_4^{3-} was precipitated with a low-valent metal, forming a Ca-P compound. In the experiments, $CaCl_2$ (solution) was added as a calcium source and the optimal molar ratio of Ca to P was 1.5 (Petzet et al., 2011). Finally, Al^{3+}remained in the relatively pure alkaline solution, which could be utilized as a raw element to produce the second PAC-based coagulant with the brine.

2.3. Fe stripping to produce $FeCl_3$-based coagulant

Fe^{3+}stripping from acidic leachate for extraction was conducted by an organic solvent, TBP (99%). All other reagents were of analytical grade. Extraction experiments were performed also in beakers (500 ml), with magnetically stirring at 400 rpm for 15 min (25 °C). Then, mixed solution was transferred into a separatory funnel, allowing to stand for 30 min, until an oil-water interface became clear; finally, the lower part (raffinate) was drawn off from the funnel bottom and the upper part (organic solution) was remained for Fe^{3+}stripping. The concentrations of metals (without Fe) and PO_4^{3-} in the raffinate were respectively detected, and the concentration of Fe in the organic solution could be calculated by a mass balance, based on the original Fe concentration in the leachate.

Fe^{3+} in the organic solution could be stripped by either HCl (0.1–0.5%) or the brine (0.3–0.8 mol Cl^-/L) in beakers, as conducted above (400 rpm for 2–15 min at 25–50 °C). The lower part in the separatory funnel was mainly $FeCl_3$ solution to be used as a coagulant.

The performances of $FeCl_3$-based coagulants ($FeCl_3$-s1: HCl stripping and $FeCl_3$-s2: brine stripping) could be compared with a commercial $FeCl_3$-based coagulant ($FeCl_3$-c) and also another PAC-based coagulant to be produced with Al^{3+} associated with the brine, based on both P-removal and turbidity removal.

2.4. Production of the PAC-based coagulant with Al^{3+} associated with the brine

In the experiments, the brine was directly added to the remaining Al^{3+}solution as mentioned above. Polymerization of the PAC-based coagulant was tested under different working conditions. After the polymerization was completed, the solution stood for aging in a constant temperature oven (70 °C), and then the liquid PAC-based coagulant was obtained. The liquid PAC-based coagulant could be concentrated and dried to form a solid PAC-based coagulant for the characterization by infrared spectroscopy.

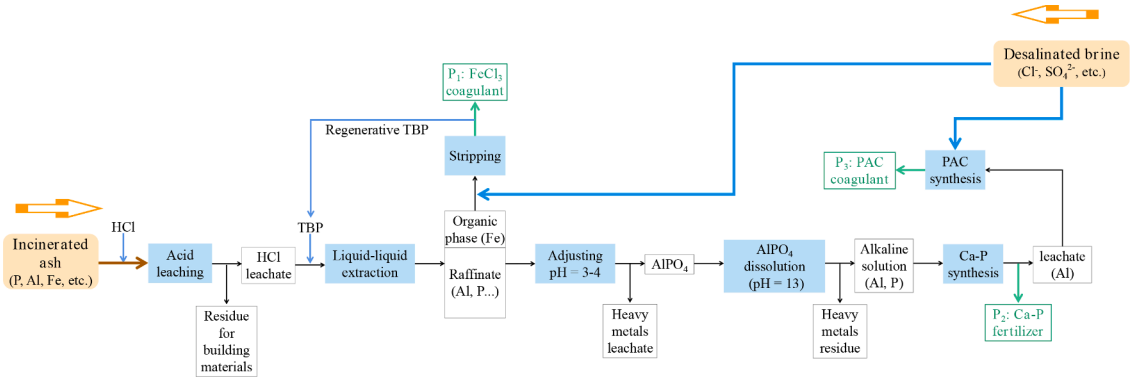

Fig. 1. Flow sheet of the study.

The performance of the liquid PAC-based coagulant (PAC-s) was compared with a commercial PAC-based (PAC-c) (Al_2O_3 wt% $\geq$ 27.0%, basicity = 45%−96%) on both P-removal and turbidity removal, based on the same Al_2O_3 concentration. The liquid PAC-based coagulant could be also compared with the $FeCl_3$-based coagulant synthetized in the first step.

2.5. Comparison of coagulation performance

Wastewater containing P was prepared with pure water as solute (PO_4^{3-} = 5 mg P/L, pH = 7.0–7.5). Effluent having turbidity was simulated with a kaolin solution (10 g of kaolin in 1 L pure water) by ultrasonic dispersion for 2 h, vigorously magnetic mixing for 6 h and sedimentation for 1 h, 800 ml; then the supernatant of the kaolin solution was diluted to 30 NTU. The coagulation experiments were conducted at 1.0 L water sample, with T = 25 °C and pH = 8.0, stirred at 500 r/min for 30 s and stirred at 100 r/min for 15 min. Finally, the stirred solution was settled for 30 min, and the turbidity of the supernatant was measured.

2.6. Analytical methods

PO_4^{3-} and metals were measured by a spectrophotometer (Cary 5000, Agilent Co., Ltd.) and inductively coupled plasma optical emission spectrometry (ICP-OES) (iCAP 7000 Series, Thermo-Fisher Co., Ltd.), respectively. The recovered Ca-P product was dissolved by aqua regia and determined for the chemical composition via ICP-OES by mass balance. The mineral phases of the Ca-P were identified by an X-ray diffractometer (XRD, DX-2700B, Dandonghaoyuan Co., Ltd., China) at 30 kV and 40 mA using Mo Kα radiation (λ = 1.54056 Å) with 2θ ranging between 5° and 90° at a scanning rate of 0.5°/min. The morphologies of the Ca-P were characterized by scanning electron microscopy (SEM, SU8020, Hitachi, Japan). The P-bioavailability was an important parameter of fertilizers, which was checked by dissolving 1 g of the Ca-P precipitate in 100 ml of 2% citric acid and stirred for 30 min (Braithwaite et al., 1989; Kratz et al., 2019; Wang et al., 2012).

The content of Al_2O_3 and the basicity on OH/Al ratio (simplified as B value) were the two main indicators to evaluate the quality of PAC-based products, which were measured according to the Chinese National Standards of water treatment chemical - poly aluminum chloride (GB 22627-2014, 2014). The chemical compositions of coagulant products were also determined via ICP-OES. The chemical functional groups were analyzed and evaluated by a Thermo Fisher Fourier transform infrared spectrometer (FT-IR). Spectra of the solid PAC products were measured at the wavenumber of 4000–400 cm^{-1} with KBr pellets (100 mg KBr + 1 mg sample, spectrum pure). The spectra of commercial $FeCl_3$ and PAC were also recorded as the standards to estimate of the quantitative similarity of chemical functional groups between the commercial coagulants and the synthesized coagulants. The mineral phases and morphologies coagulant products were also determined by XRD and SEM, respectively.

The concentrations of Cl^- and SO_4^{2-} were measured by an automatic discontinuous chemical analyzer (AQ1, SEAL Analytical, Germany). The metal elements of the desalinated brine also were measured by the ICP-OES. The turbidity of water samples before and after flocculation was measured by a turbidimeter (2100 N, HACH, America).

3. Results and discussion

3.1. Phosphate recovery as a Ca-P product

3.1.1. Chemical and mineral compositions of WAS-incinerated ash

As listed in Table 1, macro-elements in the ash were mainly Al, Ca, P, Fe and Mg; trace heavy metals were Zn, Cu, Ni, Mn and Pb, and both Cd and Cr elements were not detected, which is quite similar to literature (Liang et al., 2019). The P-element content in the ash was 10.1 wt% (23.1 wt% in P_2O_5), demonstrating that WAS-incinerated ash would become a promising secondary phosphorus source. Meanwhile, the contents of Al and Fe elements in the ash were 8.9% and 1.2%, respectively, which also reveals their value and potential on producing coagulants.

Table 1
Chemical composition of the ash detected by ICP-OES.

P (g/kg)	Al (g/kg)	Ca (g/kg)	Fe (g/kg)	Mg (g/kg)	K (g/kg)	Na (g/kg)	Cu (mg/kg)
101.3 ± 4.2	89.1 ± 3.2	46.3 ± 7.2	11.9 ± 0.4	16.5 ± 3.2	4.8 ± 3.2	7.4 ± 0.6	25.7 ± 1.9
Mn (mg/kg)	Zn (mg/kg)	Ni (mg/kg)	Pb (mg/kg)	As (mg/kg)	Cr (mg/kg)	Sn (mg/kg)	Cd (mg/kg)
16.2 ± 0.5	122.9 ± 4.6	18.3 ± 1.3	13.4 ± 5.1	ND[a]	ND	ND	ND

[a] ND: Not detected.

The SEM images of the raw ash and leaching residue are shown in Fig. S1. Particles of the ash were very rough and irregular with open pores (Fig. S1a). After leaching with HCl, acid-soluble compounds in the ash were leached out, residual ash particles were broken to small granules, still having porous morphology, loosen structure and irregular surface (Fig. S1b), as described in literature (Li et al., 2017; Liang et al., 2019). The XRD patterns and the main mineral phases of the raw ash and leaching residue are depicted in Fig. S1c. After the acidic leaching, the peak intensities of substances other than SiO_2 became weaker, which corresponded to PO_4^{3-}, Al^{3+} and Fe^{3+} obtained in the acidic leachate.

Fig. 2a reveals that the higher the acid concentration, the more P, Al, Fe, Ca and Mg extracted from the ash. When the molarity of HCl reached to 0.50 mol/L, the leaching rate of phosphorus became faster, up to 0.03 mol P/L. However, a higher acid concentration is not expected due to increased costs (Luyckx et al., 2020). The experimental results shown in Fig. 2b confirm that the higher amounts of P, Al and Fe could be extracted by increasing the L/S ratio, due to an enhanced contacting efficiency. This case was especially suitable for Fe^{3+} recovery, and the leaching efficiency increased significantly with increasing the L/S ratio from 11.1% to 90.1%. The leaching efficiency of Al^{3+} also reached to a higher ratio (94.6%) when the L/S ratio was increased to 100 ml/g. As a result, a compromise on both recovery efficiency and costs were made: 0.5 M HCl and 100 ml/g of the L/S ratio were selected as the working conditions for subsequent leaching experiments.

3.1.2. Synthesis of Ca-P product

As shown in Fig. 1, phosphate recovery from the ash consists of three main steps: i) acidic leaching of the ash; ii) extraction of Fe^{3+}; iii) precipitation and separation of Al-P and heavy metals, based on three chemical equations (Petzet et al., 2012; Semerci et al., 2020):

$$Al^{3+} + H_3PO_4 + 3OH^- \rightarrow AlPO_4\downarrow + 3H_2O \quad (1)$$

$$AlPO_4 + 4NaOH \rightarrow 4Na^+ + [Al(OH)_4]^- + PO_4^{3-} \quad (2)$$

$$3Ca^{2+} + 2PO_4^{3-} \rightarrow Ca_3(PO_4)_2\downarrow \quad (3)$$

The mass balances on P, Al, Fe and Ca during the recovery process are shown in Table S1. After the organic solvent extraction process, Fe^{3+} was extracted from the acidic leachate and finally recovered in the form of $FeCl_3$ solution. The molar ratio of Al to P was 1.06 in the raffinate, just enough to precipitate PO_4^{3-} with Al to form an Al-P compound. In addition, the remaining heavy metals were removed in the step of generating Al-P precipitation based on the SEPHOS process (Petzet et al., 2011). Finally, phosphate was recovered by adding $CaCl_2$ (Ca/P = 1.5) to form an alkaline leachate to generate the precipitation of Ca-P. Furthermore, the leachate (Residual solution III) was rich in Al^{3+} (0.28 mol/L), which was used as an Al source for synthesizing a PAC-based product in the next step.

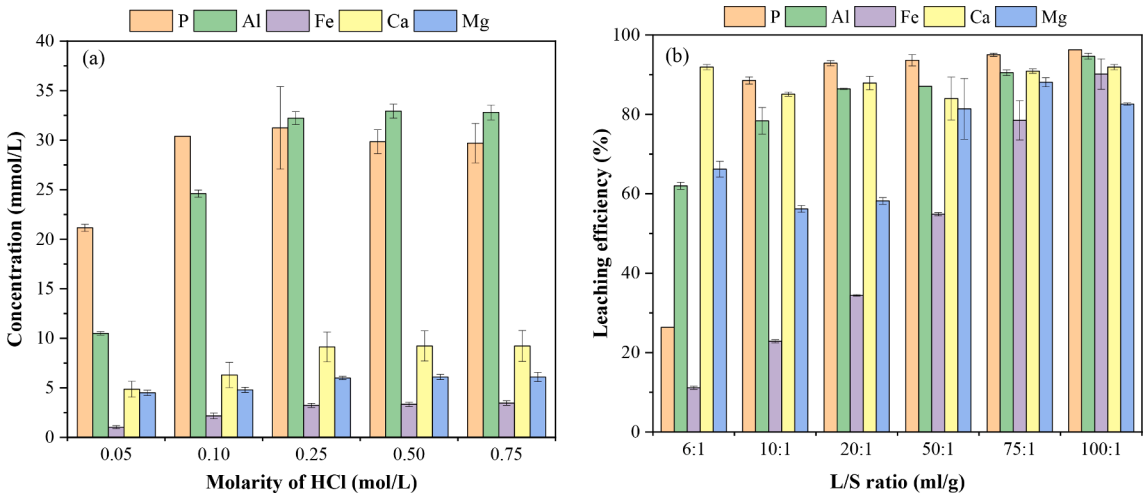

Fig. 2. Leaching of P and metal elements at different HCl concentrations (a) and liquid to solid (L/S) ratio (b) (Ash size < 500 μm, 25 ± 1 °C, 6 h; error bars represent the standard deviations, $n = 3$).

Overall, approximately 88.0 wt% of P in the ash was precipitated, and hydroxylapatite $Ca_5(PO_4)_3OH$ (HAP) was identified as the main crystal phase in the Ca-P precipitation by XRD, as depicted in Fig. S2a, which is a more versatile phosphorus fertilizer than struvite. The morphological image of the P-product is presented in Fig. S2b, indicating a relatively regular and smooth layered crystal structure. Based on the analysis on the chemical composition in Fig. 3, most of the common toxic heavy metals (Cd, Hg, Ni, Sn and Mn) in the P-product were not detected. The content of Cu, Pb and Zn was 13.2, 11.3 and 35.5 mg/kg, respectively, which were all below the limited values for fertilizer standards in most countries (Xu et al., 2012). Overall, the recovered P-compound had a high phosphorus content (37.1 wt% in P_2O_5) and a good bioavailability (60.1% soluble phosphorus).

3.2. Production of $FeCl_3$-based coagulant

3.2.1. Extraction of Fe^{3+}

Organic solvent extraction of Fe^{3+} from acidic leachate in hydrochloric acid medium by TBP includes the following steps: i) Fe^{3+} and Cl^- diffuse from the main aqueous phase to the two-phase interface, respectively; ii) TBP molecule diffuses from the organic phase to the two-phase interface; iii) a chemical reaction occurs at the interface to generate an extract that diffuses from the interface to the main body of the organic phase. The liquid-liquid extraction system is a complex extraction of neutral molecules composed of neutral organic phosphorus and high-concentration hydrochloric acid. The following two reaction Eqs. (4) and (5) represent the solvent extraction of Fe^{3+} from chloride solutions with TBP according to the different concentrations of H^+ and Cl^- (Yi et al., 2020):

$$Fe^{3+}_{(A)} + 3Cl^-_{(A)} + mTBP_{(O)} \rightarrow FeCl_3{\cdot}mTBP_{(O)} \quad (4)$$

$$Fe^{3+}_{(A)} + 4Cl^-_{(A)} + H^+ + 2TBP_{(O)} \rightarrow HFeCl_4{\cdot}2TBP_{(O)} \quad (5)$$

The extraction efficiency (E) and distribution coefficient (D) are provided as Eqs. (6) and (7), respectively.

$$E = \frac{V_{Org.}C_{Org.}}{V_F C_F} \times 100\% \quad (6)$$

$$D = \frac{C_{Org.}}{C_R} \quad (7)$$

Where, $V_{Org.}$ and V_F: the volume of organic phase and feed solution; $C_{Org.}$ or C_R: the concentration of metal in organic phase or raffinate when reaction reaches equilibrium; $C_{F:}$ the concentration of metal in feed solution.

In order to study the selectivity of TBP extractant of Fe^{3+}, the extraction experiments were carried out using the acidic leachate under the optimal acid leaching conditions (HCl = 0.5 mol/L, L/S = 100 ml/g, $T = 25 \pm 1$ °C and $t = 6$ h). The content of mainly involved elements in both the acidic leachate and raffinate is shown in Fig. 4a. One contacting stage extraction shows that TBP has a high selectivity and a good extraction ability (88.3%) for Fe^{3+}; moreover, it has no extraction ability on Al^{3+}, Ca^{2+} and Mg^{2+} (Yi et al., 2020). Although a high concentration TBP might also extract phosphorus based on some other researches (Zhang et al., 2020), the phenomenon did not happen in this study. Anyway, it is necessary to have a reasonable TBP volume fraction during Fe^{3+} extraction to avoid the loss of PO_4^{3-}. In addition, such factors as acidity of feed solution, Cl^- concentration, initial H_3PO_4 concentration and even the ratio of PO_4^{3-} and Fe^{3+}might also affect the loss rate of PO_4^{3-} during the organic solvent extraction process of Fe^{3+} by TBP (Jin et al., 2015).

The extraction effect of Fe^{3+}under different ratios of organic phase to aqueous phase (O/A) are shown in Fig. 4b. When O/A < 1.0, moreover, the third phase and emulsification are easy to appear, which made it difficult to separate, due to the low solubility of the generated complex in the organic phase (Zhang et al., 2015). At O/A > 1.0, the third phase could be avoided, but the extraction rate of $Fe^{3+}$is not improved too

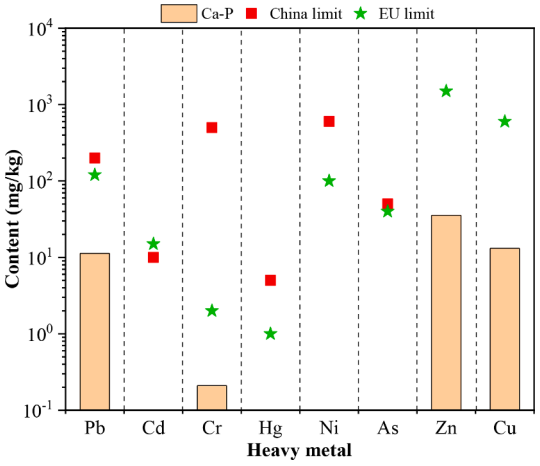

Fig. 3. Content of heavy metals associated with the precipitated Ca-P marked with the limits of China (GB 38400-2019, 2019) and EU (EC, 2019) on heavy metals for agricultural use.

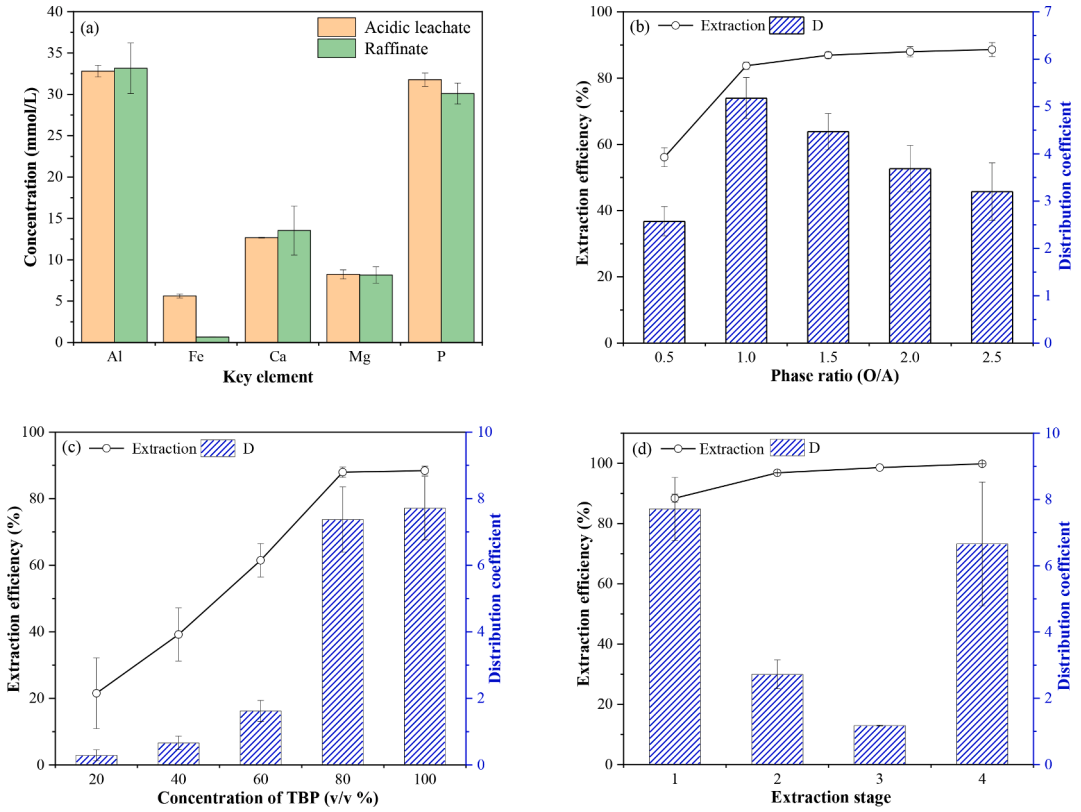

Fig. 4. Concentrations of Al^{3+}, Fe^{3+}, Ca^{2+}, Mg^{2+} and PO_4^{3-}-P in the acidic leachate and the raffinate (a); effects of phase ratio (b), the concentration of TBP (c) and the extraction stages (d) on Fe^{3+} extraction and distribution coefficient (D: distribution coefficient, calculated according to Eq. (7)) (400 rpm, 15 min, 25 ± 1 °C; error bars represent the standard deviations, $n = 3$).

much (Zhang et al., 2015) . The distribution coefficient has reached to its maximum value, 5.2 at O/A = 1.0. An even higher O/A would result in a larger equipment volume and increased operation costs, which is not conducive to the subsequent stripping and enrichment of $Fe^{3+}$for coagulant production. As a whole, the O/A ratio was selected at 1:1.

The extraction performance of different TBP concentrations in kerosene is shown in Fig. 4c. The extraction performance of Fe^{3+} increased along with increased TBP volume fraction. However, when the TBP volume fraction ranged from 80% to 100%, the distribution coefficient merely varied between 7.4 to 7.7. Moreover, the density and viscosity of the organic phase increased with increasing the TBP volume fraction, which resulted in a decrease in surface tension and a slower rate of phase disengagement (Zhang et al., 2015). Thus, the extractant consisting of 80 vol.% TBP and 20 vol.% kerosene was an effective mixed system for Fe^{3+} extraction from the acidic leachate.

The performance of TBP in kerosene is shown in Fig. 4d. The extraction performance of Fe^{3+}increased with increased stages. The two extraction stages could have recovered more than 97% of Fe^{3+}. Therefore, it was no necessary to further increase the extraction stages.

3.2.2. *$FeCl_3$ stripping*

3.2.2.1. Chemical composition of desalinated brine. As listed in Table 2, the concentrations of Cl^- and SO_4^{2-} in the brine were so high as up to 33.0 g/L and 4.1 g/L, respectively, demonstrating their applicability to be recycled as anions for producing coagulants. Besides, some main cations in the brine can also be referred in Table 2.

Table 2
Chemical composition of desalinated brine (50% water content evaporated).

Cl^- (g/L)	SO_4^{2-} (g/L)	Na^+ (g/L)	Mg^{2+} (g/L)
33.0 ± 3.2	4.1 ± 0.9	35.7 ± 9.5	2.6 ± 0.5
K^+ (g/L)	Ca^{2+} (g/L)	Li^+ (mg/L)	Br^- (g/L)
0.77 ± 0.1	0.53 ± 0.2	0.43 ± 0.1	0.14 ± 0.4

3.2.2.2. $FeCl_3$ stripping with HCl and the brine. Extraction is to extract extractable substances into the organic phase, while stripping is to strip extracted substances from the loaded organic phase. In the simple stripping process, the dilution effect of the stripping agent can reverse the extraction equilibrium, and then the extraction reaction proceeds in the reverse direction, so as to achieve the purpose of stripping. Based on the existing researches (Cohen and Enfält, 2018), HCl has been identified as being the most effective stripping agent for the Fe^{3+}-loaded TBP (Azizitorghabeh et al., 2017; Saji and Reddy, 2001). Similarly, desalinated brine could be used as a novel stripping agent for Fe^{3+} stripping, which was trialed in this study as a comparison with HCl. Among others, the stripping efficiency (S) is presented in Eq. (8). $V'_{Aq.}$ and $C'_{Aq.}$ are respectively the volume and the metal concentration of stripping aqueous phase.

$$S = \frac{V'_{Aq.}C'_{Aq.}}{V_{Org.}C_{Org.}} \times 100\% \quad (8)$$

In order to obtain the optimal stripping conditions (O/A, temperature, Cl^-/HCl concentration and time), the experiments were carried out using the loaded organic phase under optimal the one-stage extraction condition (80%TBP and O/A = 1:1), and the results were showed in Fig. 5. According to Fig. 5a, O/A suitable for Fe^{3+} stripping was determined at 2:1. With increasing O/A from 1.0 to 5.0, the Fe^{3+}stripping efficiency tended to quickly take off and then slowly descend. Between O/A = 1.0–2.0, the stripping efficiency of HCl and the brine both increased from 79.6% to 91.1% and 71.4% to 87.5%, respectively. At O/A = 2.0–5.0, conversely, the stripping efficiency significantly decreased

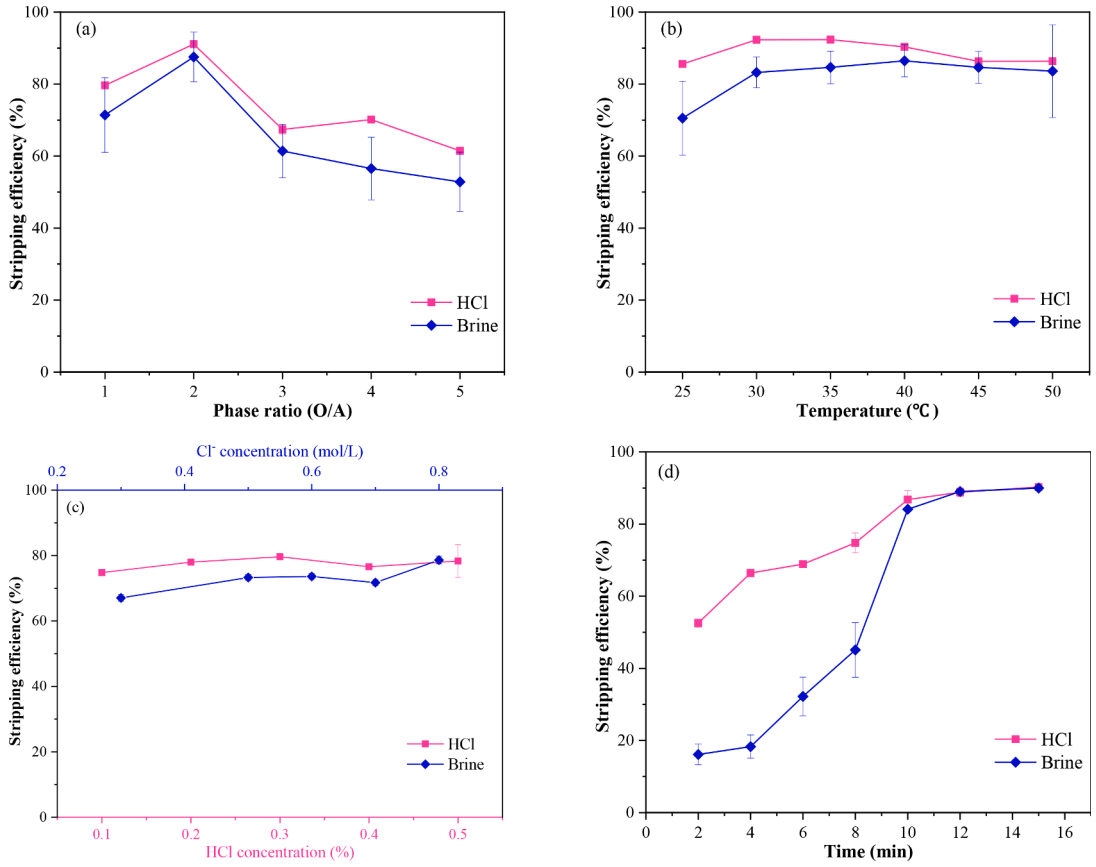

Fig. 5. Effects of phase ratio (a), temperature (b), HCl or Cl^- concentration (c) and time (d) on Fe^{3+} stripping (400 rpm; error bars represent the standard deviations, $n = 3$).

even though Fe^{3+} was further concentrated. In a word, the brine had almost the same stripping efficiency as HCl, which could be used as a stripping agent to produce $FeCl_3$ coagulant. According to Fig. 5b, clearly, the stripping could be carried out at 25 °C or room temperature for saving operation cost. The two striping agents were endothermic and had the same temperature-dependent trend. However, the stripping efficiency did not further increase after 35–40 °C, as the organic phase might volatilize at high temperature.

According to Fig. 5c, the optimal concentrations of HCl and Cl^- were determined at 0.3% and 0.5 mol/L, respectively. With increasing the concentration of HCl or Cl^-, the two stripping agents had a similar tendence on slightly improving the stripping efficiency. Based on Eqs. (4) and (5), the dilution of the stripping agent can make the reaction proceed in the reverse direction, while increasing the concentration of HCl or Cl^- is not conductive to the reverse progress of the reaction; the lower the acidity, the easier the stripping. If the acidity of the stripping solution is too low, however, it is easy to cause $Fe^{3+}$to be hydrolyzed in the stripping solution, which would make the stripping solution turbid and difficult for phase separation (Zhang et al., 2015). In order to avoid introducing excessive salt in $FeCl_3$-s2, the lower Cl^- concentration should be used. Finally, the proper time for stripping was set up at 15 min according to Fig. 5d, because the stripping efficiency of HCl and the brine became almost same and maximum in 12 min.

3.2.3. *Characteristics of $FeCl_3$ product*

According to the representative IR spectrum of TBP and Fe^{3+}-loaded organic phase shown in Fig. S3a, the peak around 1280 cm^{-1} was assigned to the $P = O$ bands, which was highly affected when the organic phase interacted with Fe^{3+}. The $P = O$ band stretching vibration at 1280 cm^{-1} in TBP was shifted to 1270 cm^{-1}. This was because of the high affinity of oxygen of the $P = O$ ligands of both organic solvent molecules for Fe^{3+} ($P = O \rightarrow Fe^{3+}$) and the addition of $FeCl_4^-$ complex ions to P atom, restricting the $P = O$ vibration (Azizitorghabeh et al., 2016; Zhang et al., 2015). According to Fig. S3b, the solid $FeCl_3$-s1 and $FeCl_3$-s2 product should be an analog of $FeCl_3 \bullet 6H_2O$. As shown in Figs. S3c-e (the morphological images), the irregular surfaces of $FeCl_3$-c, $FeCl_3$-s1 and $FeCl_3$-s2 were similar, although the latter had a larger surface particle. Moreover, the EDS analysis in Fig. S3f on $FeCl_3$-s2 confirmed its chemical composition, consisting of Fe, Cl, Na, Mg, K, Ca and O, which could be speculated as $FeCl_3$.

3.3. *Al recovered for PAC-based coagulant*

PAC contains different amounts of hydroxyl, and the empirical molecular formula is $[Al_m(OH)_n(H_2O)_x]\cdot Cl_{3m-n}$ ($0 < n \leq 3$ m) (Li et al., 2010). The chemical reaction during the formation of PAC is presented in Eq. (9) (Guo et al., 2022). A gradually increasing pH can promote the hydrolysis of Al^{3+}. When pH increases to a certain value, bridging polymerization occurs between the two adjacent OH^- (Zhao et al., 2009, 2012). Along with the polymerization progress, the concentration of the hydrolyzate decreases, thereby prompting the hydrolysis to proceed (Li et al., 2010; Tang et al., 2015). During the polymerization reaction, the hydrolysis and polymerization of Al^{3+} are carried out alternately, so that the reaction develops in the direction of forming a hydroxylated flocculant with a high Al_2O_3 content, a high B value, and a high degree of polymerization. By controlling the polymerization conditions well, a PAC solution with the qualified Al_2O_3 content and B value could be obtained.

The leachate (Residual solution III) was used as the Al^{3+} source for PAC-based production, and the anion of Cl^- from the brine was added at a molar ratio of Al/Cl^- at 1:3, and then the mixed solution was used to explore the optimal conditions for the polymerization, including pH,

temperature and time.

$$2AlCl_3+nNaOH \xrightarrow{\Delta} Al_2(OH)_nCl_{6-n}+nNaCl \quad (9)$$

3.3.1. Synthesis of PAC-based coagulant

The polymerization pH of the mixed solution containing Al^{3+} from the ash and Cl^- from the brine was a key factor to synthesize PAC-based coagulant. At the polymerization temperature (T) of 70 °C and the polymerization time (t) for 2 h, the relationship of the polymerization pH and the PAC content (calculated by Al_2O_3, w/w) as well as the *B* value of PAC-based coagulant were investigated, as shown in Fig. 6a. At pH < 3.0, there were too many free acids in the mixed solution, which would inhibit the hydrolysis of hydrated aluminum ions and then the degree of polymerization and the *B* value was too low, which could ultimately affect the coagulation effect of PAC-based coagulant. At pH > 3, the aluminum hydroxide colloid was easily generated in the mixed solution and PAC-based coagulant was difficult to exist stably, resulting in a rapid decrease in the content of Al_2O_3. Clearly, pH was significantly related to the degree of hydrolysis of Al^{3+} in the mixed solution, and pH = 3.0 should be appropriate for subsequent experiments.

The polymerization temperature also has an important influence on the formation of PAC. At pH = 3.0 and t = 2 h, the results of temperature-dependent polymerization are shown in Fig. 6b. At T = 70 °C, both Al_2O_3 content and *B* value reached up to their maximal data, at 3.7% and 69.4%, respectively. When T < 70 °C, the reaction was not sufficient, and the time to form the polymer had to be long, resulting in a long reaction and a low degree of polymerization. However, the hydrolysis process of $Al^{3+}$is an endothermic process. As a result, a higher than 70 °C would cause the structure and stability of the polymerized state destroyed, resulting in the decomposition of a part of the polymer and the formation of $Al(OH)_3$ precipitation. For this reason, 70 °C was fixed for subsequent experiments.

At pH = 3.0 and T = 70 °C, the results of the polymerization time vs. both Al_2O_3 content and *B* value are shown in Fig. 6c. There was the best polymerization time for the *B* value and also the Al_2O_3 content, at t = 2 h. As a result, the optimal reaction conditions of the polymerization of PAC-based coagulant could be determined at pH = 3.0, T = 70 °C and t = 2 h.

3.3.2. Characteristics of PAC-based coagulant

The commercial PAC (PAC-c) was used as a counterpart to compare the characteristics of PAC-s. The FT-IR spectrum (Fig. 7a) in the range of 4000–400 cm^{-1} reveals that two main absorption peaks were quite similar to each other. Among them, the absorption peaks at 1093 and 1100 cm^{-1} were the stretching vibration peaks of Al-OH-Al, indicating an aggregation state (Guo et al., 2022). Moreover, the absorption peaks near 870 cm^{-1} were the in-plane flexural vibration peak of Al-OH-Al, which reflects the bonding between aluminum atoms through oxygen bridges in the process of reconversion of aluminum chloride to PAC (Tzoupanos et al., 2009). Finally, the strong absorption peaks at 700–400 cm^{-1} were the overall flexural vibration absorption peak of Al-OH superimposed on the absorption peaks of water molecules, which also indicates that the PAC-s molecules contained hydroxyl and polymeric aluminum (Tzoupanos and Zouboulis, 2011). Therefore, the synthesized compound could be confirmed to be a PAC-based product.

Based on Fig. 7b, there was no diffraction peak of $AlCl_3$ in the XRD pattern of the PAC-s, indicating that Al^{3+}, Cl^- and hydroxyl structure (-OH) reacted to form an amorphous polymer. Compared with the powder diffraction file (PDF) card (no.: 96–430–0181), the diffraction peaks at 31.6° and 45.5° were the characteristic peaks of sodium chloride (Tang et al., 2015). The crystallinity of sodium chloride was good, which masked the diffraction peaks of the amorphous polymer (Tzoupanos and Zouboulis, 2011). More sodium chloride was generated in PAC-s, which was formed by the combination of Na^+ in NaOH and Cl^- in the brine. In contrast, the XRD pattern of PAC-c revealed an amorphous shape, which was related to the fact that it is derived from a commercial synthetic process and contains less sodium chloride. As shown in Fig. 7c (the morphological image), the surface of PAC-s was smooth with small wrinkles, which was consistent with the results in the literature (Guo et al., 2022).

The chemical composition of the solid PAC-s and the solid PAC-c was listed in Table S2. The impurity metal ions were mainly consisted of Na and Mg, but the contents of them were at < 6.0%, which could cause little impact on wastewater treatment. Furthermore, these impurities could be purified in a further study by extracting Cl^- from the brine.

3.4. Coagulation performance

3.4.1. $FeCl_3$-based coagulant

The coagulation performance of the synthesized $FeCl_3$ ($FeCl_3$-s1 and $FeCl_3$-s2) was compared with a commercial $FeCl_3$ ($FeCl_3$-c) in P-removal (a) and turbidity (b) removal, as shown in Fig. 8. In the dosing rage of 10–50 mg/L (Fe/P = 1.11–5.54), the P-removal efficiency increased from 16.1% to 95.4% ($FeCl_3$-c), 15.2% to 93.0% ($FeCl_3$-s1) and 14.1% to 88.1% ($FeCl_3$-s2), respectively, demonstrating the almost same P-removal ability of $FeCl_3$-s1 and $FeCl_3$-s2 as $FeCl_3$-c (Fig. 8a).

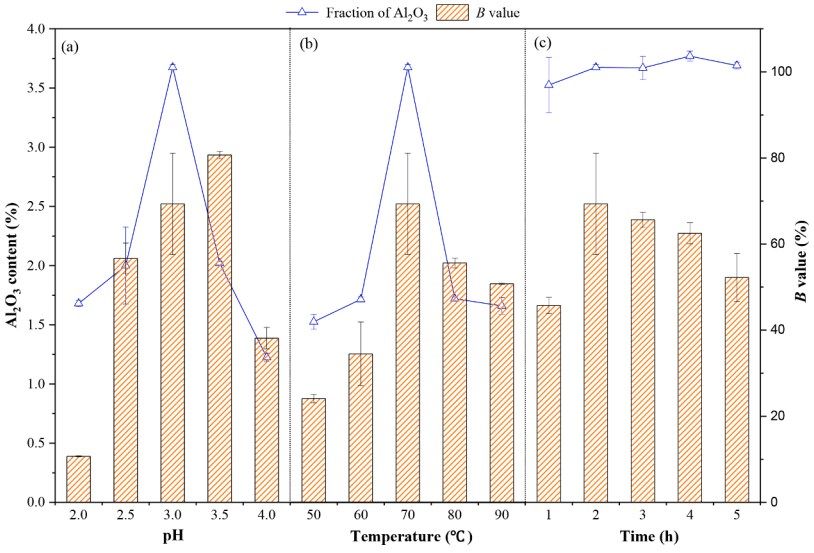

Fig. 6. Effects of the polymerization pH (a), temperature (b), time (c) on PAC synthesis (Error bars represent the standard deviations, n = 3).

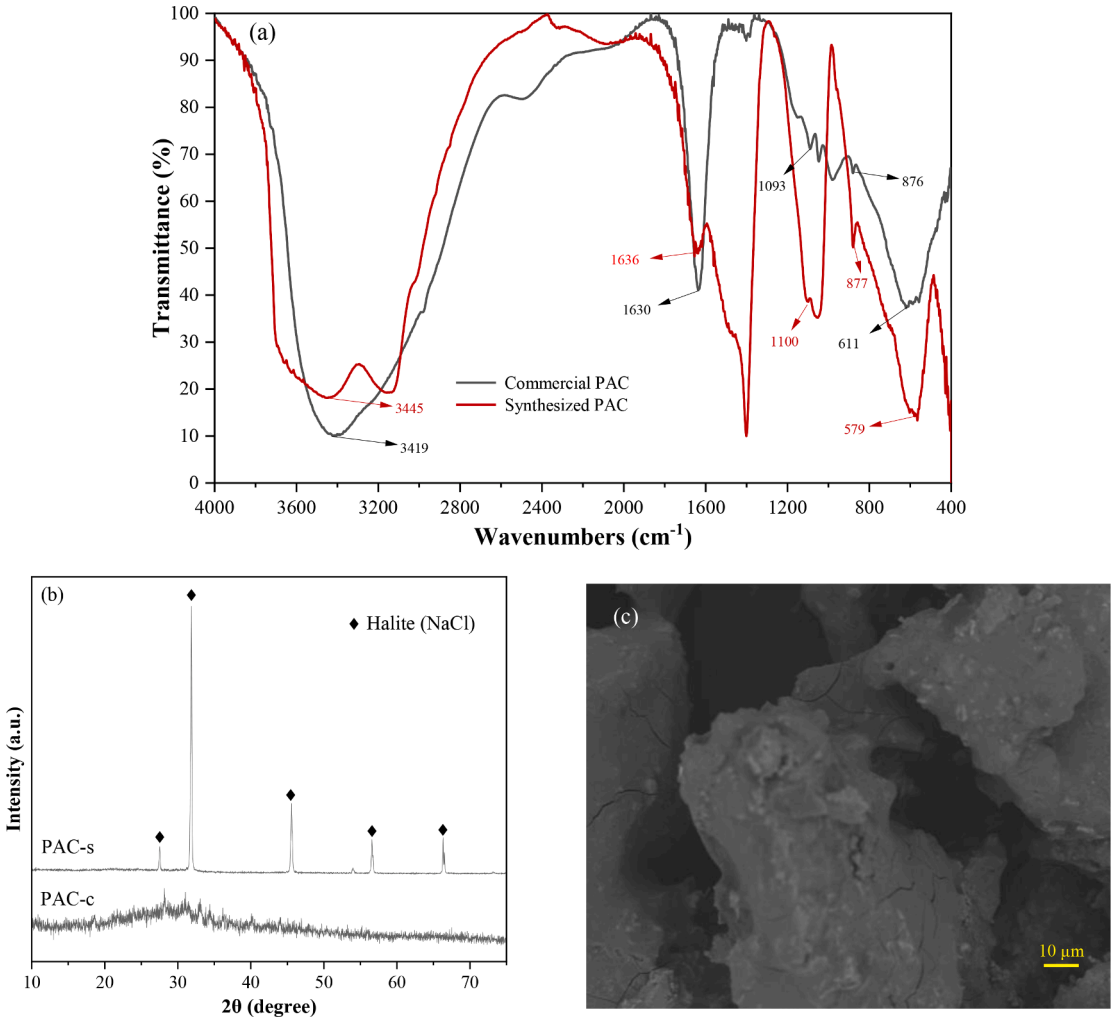

Fig. 7. FT-IR spectrum (a), XRD-analyses (b) and SEM image (c) (magnification 500 times) of PAC-s and PAC-c.

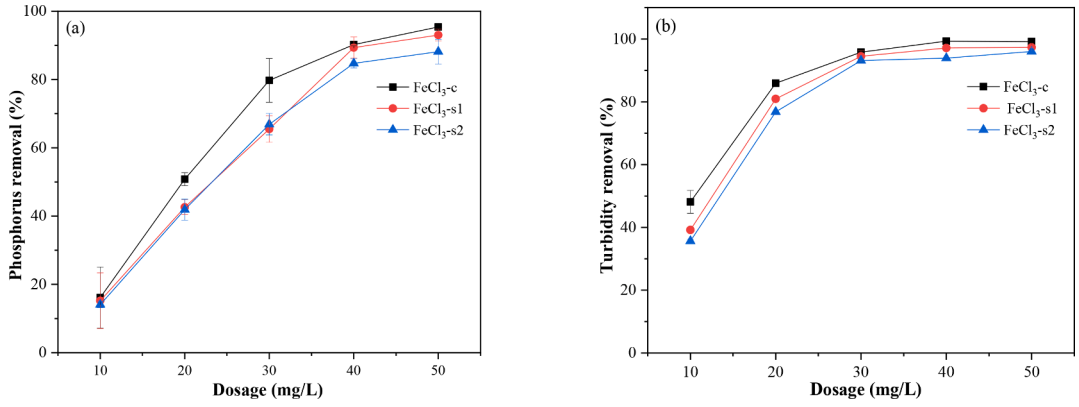

Fig. 8. Coagulation comparison of the synthesized $FeCl_3$ ($FeCl_3$-s1 stripped with HCl and $FeCl_3$-s2 stripped with the brine) with the commercial $FeCl_3$ ($FeCl_3$-c) in P-removal (a) and turbidity (b) removal (Initial PO_4^{3-} = 5 mg P/L, initial turbidity = 30 NTU, 1.0 L water sample, 25 ± 1 °C, pH = 8.0, 500 rpm for 30 s, 100 rpm for 15 min; error bars represent the standard deviations, n = 3).

Similarly, the turbidity removal of $FeCl_3$-s1 and $FeCl_3$-s2 had also the same ability as $FeCl_3$-c (Fig. 8b), from 48.1% to 99.2% ($FeCl_3$-c), 39.2% to 97.3% ($FeCl_3$-s1) and 35.6% to 96.0% ($FeCl_3$-s2), respectively. The experiments revealed that $FeCl_3$-s2 with the brine as the stripping agent could be used as a potential coagulant at least in wastewater treatment.

3.4.2. *PAC-based coagulant*

Both PAC-c and PAC-s were added to the solutions with the same mass concentration to compare their performances in P-removal (Fig. 9a) and turbidity removal (Fig. 9b). At the same time, $FeCl_3$-s2 in the same performances were also put in Fig. 9. As shown in Fig. 9, PAC-s had more or less the same trend and magnitude on two removal efficiencies as PAC-c in the dosage range of 10–35 mg/L. At 35 mg/L (Al/*P*

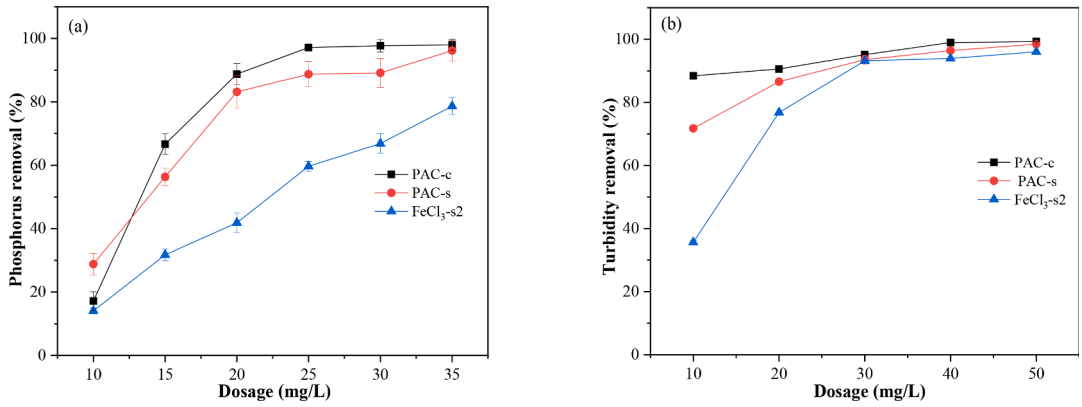

Fig. 9. Coagulation performance of the synthesized PAC (PAC-s), $FeCl_3$ ($FeCl_3$-s2) and the commercial PAC (PAC-c) on P-removal (a) and turbidity removal (b) (Initial PO_4^{3-} = 5 mg P/L, initial turbidity = 30 NTU, 1.0 L water sample, 25 ± 1 °C, pH = 8.0, 500 rpm for 30 s, 100 rpm for 15 min; error bars represent the standard deviations, n = 3).

= 4.25) dosed, the P-concentration after removal could reach down to < 0.2 mg P/L from initial 5 mg P/L, and the turbidity after removal could be decreased to 0.46 NTU from initial 30 NTU. Moreover, the concentration of TDS even in the dosage concentration of 50 mg/L PAC-s was also low (473 mg/L), much less than 1500 mg/L limited for non-drinking use in China. By contrast, $FeCl_3$-s2 behaved weak in the same performances, which implies that $FeCl_3$-based coagulant seems unnecessary to be produced from the point of practical view.

Moreover, synthesized coagulants could completely save the costs of buying raw materials and disposing wasted metals and brine. So the production cost of synthesized coagulants can be expected to be much lower than commercial coagulants, under the same process of coagulant production (transportation should keep equal).

3.4.3. *Outlook and prospect*

The synergy of WAS-incinerated ash and desalinated brine could both recover phosphate and produce coagulants/flocculants, towards the circular/blue economy. P-recovery from wastewater/sludge has become a global activity, and consumption on coagulants for water/wastewater treatment is becoming more and more, especially in China (the largest consumer of coagulants in the world). In the future, we also could use the new absorbent for directly recovering P from the acid leachate, which could further reduce the cost of P-recovery (Kajjumba et al., 2021; Yu et al., 2021). Moreover, incineration will gradually become a main-stream approach to handling waste activated sludge domestically and globally (Hao et al., 2020b), and thus the best stie of P-recovery can be expected from WAS-incinerated ash (Hao et al., 2013). It can be imagined that both P-recovery from the ash and synergized coagulant production with the brine would enlarge the market of both 'blue' phosphate and 'green' coagulants.

4. Conclusions

With a synergic concept, phosphate recovery from WAS-incinerated ash and coagulant production associated with desalinated brine were trialed, mainly related to P, Al and Fe in the ash and Cl^- and SO_4^{2-} in the brine. After the experiments, some main conclusions can be drawn below:

- With acid (HCl) leaching and metals' removing, approximately 88.0 wt% of phosphorus (P) in the ash could be recovered as hydroxylapatite (HAP: $Ca_5(PO_4)_3OH$).
- Fe^{3+} in the acidic leachate could be selectively removed/recovered by the organic solvent (TBP) extraction, and $FeCl_3$-based coagulant could be obtained simply by stripping the raffinate with the original brine.
- A liquid PAC-based coagulant could be synthesized with Al^{3+} removed from the ash and the original brine, which has a comparable chemical structure and coagulation performance with a commercial PAC.
- The liquid PAC-based coagulant had almost the same performances on both phosphate and turbidity removals as a commercial coagulant. However, the synergized $FeCl_3$-based coagulant behaved weak in the same performances.
- Both P-recovery from the ash and synergized coagulant production with the brine would enlarge the market of both 'blue' phosphate and 'green' coagulants.

Declaration of Competing Interest

The authors declare that they have no known competing financial interests or personal relationships that could have appeared to influence the work reported in this paper.

Data availability

Data will be made available on request.

Acknowledgements

The study was financially supported by the National Natural Science Foundation of China (52170018), and the Scientific Research Project of Beijing Municipal Education Commission (KM202210016007).

Supplementary materials

Supplementary material associated with this article can be found, in the online version, at doi:10.1016/j.watres.2023.119658.

References

Azizitorghabeh, A., Rashchi, F., Babakhani, A., 2016. Stoichiometry and structural studies of Fe(III) and Zn(II) solvent extraction using D2EHPA/TBP. Sep. Purif. Technol. 171, 197–205. https://doi.org/10.1016/j.seppur.2016.07.037.

Azizitorghabeh, A., Rashchi, F., Babakhani, A., Noori, M., 2017. Synergistic extraction and separation of Fe(III) and Zn(II) using TBP and D2EHPA. Sep. Sci. Technol. 52, 476–486. https://doi.org/10.1080/01496395.2016.1250778.

Boniardi, G., Turolla, A., Fiameni, L., Gelmi, E., Malpei, F., Bontempi, E., Canziani, R., 2021. Assessment of a simple and replicable procedure for selective phosphorus recovery from sewage sludge ashes by wet chemical extraction and precipitation. Chemosphere 285, 131476. https://doi.org/10.1016/j.chemosphere.2021.131476.

Braithwaite, A.C., Eaton, A.C., Groom, P.S., 1989. Some factors associated with the use of the extractants 2% citric acid and 2% formic acid as estimators of available phosphorus in fertiliser products. Fertil. Res. 19, 175–181. https://doi.org/10.1007/BF01054459.

Chrispim, M.C., Scholz, M., Nolasco, M.A., 2019. Phosphorus recovery from municipal wastewater treatment: critical review of challenges and opportunities for developing countries. J. Environ. Manage. 248, 109268 https://doi.org/10.1016/j.jenvman.2019.109268.

Cohen, Y., Enfält, P., 2018. Production of phosphate compounds from materials containing phosphorus and at least one of iron and aluminium. Patent US 10, 023,464 B2.

Deep, A., Correia, P.F.M., De Carvalho, J.M.R., 2007. Liquid-liquid extraction and separation of a macro concentration of Fe $^{3+}$. Ind. Eng. Chem. Res. 46, 5707–5714. https://doi.org/10.1021/ie0615279.

EC, 2019. European Council. Regulation (EU) 2019/of the European Parliament and of the Council of 5 June 2019 Laying Down Rules on the Making Available on the Market of EU Fertilising Products and Amending Regulations (EC) no 1069/2009 and (EC) no 1107/2009 and Repealing Regulation (EC) no 2003/2003. p. 114. http://data.europa.eu/eli/reg/2019/1009/oj.

Fahimi, A., Federici, S., Depero, L.E., Valentim, B., Vassura, I., Ceruti, F., Cutaia, L., Bontempi, E., 2021. Evaluation of the sustainability of technologies to recover phosphorus from sewage sludge ash based on embodied energy and CO_2 footprint. J. Clean. Prod. 289, 125762 https://doi.org/10.1016/j.jclepro.2020.125762.

Fang, L., Wang, Q., Li, J.shan, Poon, C.S., Cheeseman, C.R., Donatello, S., Tsang, D.C.W., 2020. Feasibility of wet-extraction of phosphorus from incinerated sewage sludge ash (ISSA) for phosphate fertilizer production: a critical review. Crit. Rev. Environ. Sci. Technol. 0, 1–33. https://doi.org/10.1080/10643389.2020.1740545.

Galey, B., Gautier, M., Kim, B., Blanc, D., Chatain, V., Ducom, G., Dumont, N., Gourdon, R., 2022. Trace metal elements vaporization and phosphorus recovery during sewage sludge thermochemical treatment – A review. J. Hazard. Mater. https://doi.org/10.1016/j.jhazmat.2021.127360.

GB 22627-2014, 2014. Water Treatment Chemical-Poly Aluminium Chloride. Standards Press of China. Beijing (in Chinese).

GB 38400-2019, 2019. Limitation Requirements of Toxic and Harmful Substance in Fertilizers. Standards Press of China. Beijing (in Chinese).

Geng, H., Xu, Y., Zheng, L., Gong, H., Dai, L., Dai, X., 2020. An overview of removing heavy metals from sewage sludge: achievements and perspectives. Environ. Pollut. 266, 115375 https://doi.org/10.1016/j.envpol.2020.115375.

Guo, J., Zhou, Z., Ming, Q., Huang, Z., Zhu, J., Zhang, S., Xu, J., Xi, J., Zhao, Q., Zhao, X., 2022a. Recovering precipitates from dechlorination process of saline wastewater as poly aluminum chloride. Chem. Eng. J. 427, 131612 https://doi.org/10.1016/j.cej.2021.131612.

Guo, Y., Li, X., Sun, J., Liu, Y., Wang, H., Ding, J., Chen, L., Tian, X., Yuan, Y., 2022b. Physicochemical characterization and flocculation performance evaluation of PAC/PMAPTAC composite flocculant. J. Appl. Polym. Sci. 139, 51653. https://doi.org/10.1002/app.51653.

Hao, X., Chen, Q., van Loosdrecht, M.C.M., Li, J., Jiang, H., 2020a. Sustainable disposal of excess sludge: incineration without anaerobic digestion. Water Res. 170 https://doi.org/10.1016/j.watres.2019.115298.

Hao, X., Chen, Q., van Loosdrecht, M.C.M., Li, J., Jiang, H., 2020b. Sustainable disposal of excess sludge: incineration without anaerobic digestion. Water Res. https://doi.org/10.1016/j.watres.2019.115298.

Hao, X., Wang, C., Van Loosdrecht, M.C.M., Hu, Y., 2013. Looking beyond struvite for P-recovery. Environ. Sci. Technol. https://doi.org/10.1021/es401140s.

Hao, X., Wang, X., Shi, C., van Loosdrecht, M.C.M., Wu, Y., 2022a. Creating coagulants through the combined use of ash and brine. Sci. Total Environ. 845, 157344 https://doi.org/10.1016/j.scitotenv.2022.157344.

Hao, X., Yu, W., Yuan, T., Wu, Y., van Loosdrecht, M.C.M., 2022b. Unravelling key factors controlling vivianite formation during anaerobic digestion of waste activated sludge. Water Res. 223, 118976 https://doi.org/10.1016/j.watres.2022.118976.

Jin, Y., Zou, D., Wu, S., Cao, Y., Li, J., 2015. Extraction kinetics of phosphoric acid from the phosphoric acid - calcium chloride solution by tri-n-butyl phosphate. Ind. Eng. Chem. Res. 54, 108–116. https://doi.org/10.1021/ie503273j.

Jones, E., Qadir, M., van Vliet, M.T.H., Smakhtin, V., Kang, S.mu, 2019. The state of desalination and brine production: a global outlook. Sci. Total Environ. https://doi.org/10.1016/j.scitotenv.2018.12.076.

Jupp, A.R., Beijer, S., Narain, G.C., Schipper, W., Slootweg, J.C., 2021. Phosphorus recovery and recycling – closing the loop. Chem. Soc. Rev. 50, 87–101. https://doi.org/10.1039/D0CS01150A.

Kajjumba, G.W., Fischer, D., Risso, L.A., Koury, D., Marti, E.J., 2021. Application of cerium and lanthanum coagulants in wastewater treatment—a comparative assessment to magnesium, aluminum, and iron coagulants. Chem. Eng. J. 426, 131268 https://doi.org/10.1016/j.cej.2021.131268.

Kratz, S., Vogel, C., Adam, C., 2019. Agronomic Performance of P recycling Fertilizers and Methods to Predict it: a review, Nutrient Cycling in Agroecosystems. Springer, Netherlands. https://doi.org/10.1007/s10705-019-10010-7.

Li, F., Jiang, J.Q., Wu, S., Zhang, B., 2010. Preparation and performance of a high purity poly-aluminum chloride. Chem. Eng. J. 156, 64–69. https://doi.org/10.1016/j.cej.2009.09.034.

Li, J.shan, Tsang, D.C.W., Wang, Q.ming, Fang, L., Xue, Q., Poon, C.S., 2017. Fate of metals before and after chemical extraction of incinerated sewage sludge ash. Chemosphere 186, 350–359. https://doi.org/10.1016/j.chemosphere.2017.08.012.

Liang, S., Chen, H., Zeng, X., Li, Z., Yu, W., Xiao, K., Hu, J., Hou, H., Liu, B., Tao, S., Yang, J., 2019. A comparison between sulfuric acid and oxalic acid leaching with subsequent purification and precipitation for phosphorus recovery from sewage sludge incineration ash. Water Res. 159, 242–251. https://doi.org/10.1016/j.watres.2019.05.022.

Liu, H., Hu, G., Basar, I.A., Li, J., Lyczko, N., Nzihou, A., Eskicioglu, C., 2021. Phosphorus recovery from municipal sludge-derived ash and hydrochar through wet-chemical technology: a review towards sustainable waste management. Chem. Eng. J. 417, 129300 https://doi.org/10.1016/j.cej.2021.129300.

Liu, Y., Qu, H., 2016. Design and optimization of a reactive crystallization process for high purity phosphorus recovery from sewage sludge ash. J. Environ. Chem. Eng. 4, 2155–2162. https://doi.org/10.1016/j.jece.2016.03.042.

Luyckx, L., Geerts, S., Van Caneghem, J., 2020. Closing the phosphorus cycle: multi-criteria techno-economic optimization of phosphorus extraction from wastewater treatment sludge ash. Sci. Total Environ. 713, 135543 https://doi.org/10.1016/j.scitotenv.2019.135543.

Ma, P., Rosen, C., 2021. Land application of sewage sludge incinerator ash for phosphorus recovery: a review. Chemosphere 274, 129609. https://doi.org/10.1016/j.chemosphere.2021.129609.

Morf, L., Schlumberger, S., Adam, F., Díaz Nogueira, G., 2019. Urban phosphorus mining in the canton of Zurich: phosphoric acid from sewage sludge ash, in: phosphorus recovery and recycling. pp. 157–177. https://doi.org/10.1007/978-981-10-8031-9_10.

Ortiz-Albo, P., Torres-Ortega, S., González Prieto, M., Urtiaga, A., Ibañez, R., 2019. Techno-economic feasibility analysis for minor elements valorization from desalination concentrates. Sep. Purif. Rev. 48, 220–241. https://doi.org/10.1080/15422119.2018.1470537.

Pérez-González, A., Ibáñez, R., Gómez, P., Urtiaga, A.M., Ortiz, I., Irabien, J.A., 2015. Nanofiltration separation of polyvalent and monovalent anions in desalination brines. J. Memb. Sci. 473, 16–27. https://doi.org/10.1016/j.memsci.2014.08.045.

Petzet, S., Peplinski, B., Bodkhe, S.Y., Cornel, P., 2011. Recovery of phosphorus and aluminium from sewage sludge ash by a new wet chemical elution process (SESAL-Phos-recovery process). Water Sci. Technol. 64, 693–699. https://doi.org/10.2166/wst.2011.682.

Petzet, S., Peplinski, B., Cornel, P., 2012. On wet chemical phosphorus recovery from sewage sludge ash by acidic or alkaline leaching and an optimized combination of both. Water Res. 46, 3769–3780. https://doi.org/10.1016/j.watres.2012.03.068.

Pistocchi, A., Bleninger, T., Breyer, C., Caldera, U., Dorati, C., Ganora, D., Millán, M.M., Paton, C., Poullis, D., Herrero, F.S., Sapiano, M., Semiat, R., Sommariva, C., Yuece, S., Zaragoza, G., 2020. Can seawater desalination be a win-win fix to our water cycle? Water Res. 182, 115906 https://doi.org/10.1016/j.watres.2020.115906.

Prot, T., Korving, L., Dugulan, A.I., Goubitz, K., van Loosdrecht, M.C.M., 2021. Vivianite scaling in wastewater treatment plants: occurrence, formation mechanisms and mitigation solutions. Water Res. 197, 117045 https://doi.org/10.1016/j.watres.2021.117045.

Qi, L., Liu, K., Wang, R., Li, J., Zhang, Y., Chen, L., 2020. Removal of chlorine ions from desulfurization wastewater by modified fly ash hydrotalcite. ACS Omega 5, 31665–31672. https://doi.org/10.1021/acsomega.0c04074.

Saji, J., Reddy, M.L.P., 2001. Liquid-liquid extraction separation of iron(III) from titania wastes using TBP-MIBK mixed solvent system. Hydrometallurgy 61, 81–87. https://doi.org/10.1016/S0304-386X(01)00146-3.

Semerci, N., Ahadi, S., Coşgun, S., 2020. Comparison of dried sludge and sludge ash for phosphorus recovery with acidic and alkaline leaching. Water Environ. J. 1–12. https://doi.org/10.1111/wej.12633.

Smol, M., Adam, C., Anton Kugler, S., 2020. Inventory of Polish municipal sewage sludge ash (SSA) – mass flows, chemical composition, and phosphorus recovery potential. Waste Manag 116, 31–39. https://doi.org/10.1016/j.wasman.2020.07.042.

Tang, X., Zheng, H., Teng, H., Zhao, C., Wang, Y., Xie, W., Chen, W., Yang, C., 2015. An alternative method for preparation of polyaluminum chloride coagulant using fresh aluminum hydroxide gels: characterization and coagulation performance. Chem. Eng. Res. Des. 104, 208–217. https://doi.org/10.1016/j.cherd.2015.08.009.

Tzoupanos, N.D., Zouboulis, A.I., 2011. Preparation, characterisation and application of novel composite coagulants for surface water treatment. Water Res. 45, 3614–3626. https://doi.org/10.1016/j.watres.2011.04.009.

Tzoupanos, N.D., Zouboulis, A.I., Tsoleridis, C.A., 2009. A systematic study for the characterization of a novel coagulant (polyaluminium silicate chloride). Colloids Surfaces A Physicochem. Eng. Asp. 342, 30–39. https://doi.org/10.1016/j.colsurfa.2009.03.054.

van der Kooij, S., van Vliet, B.J.M., Stomph, T.J., Sutton, N.B., Anten, N.P.R., Hoffland, E., 2020. Phosphorus recovered from human excreta: a socio-ecological-technical approach to phosphorus recycling. Resour. Conserv. Recycl. https://doi.org/10.1016/j.resconrec.2020.104744.

Wang, T., Camps-Arbestain, M., Hedley, M., Bishop, P., 2012. Predicting phosphorus bioavailability from high-ash biochars. Plant Soil 357, 173–187. https://doi.org/10.1007/s11104-012-1131-9.

Wei, Q., Ren, X., Guo, J., Chen, Y., 2016. Recovery and separation of sulfuric acid and iron from dilute acidic sulfate effluent and waste sulfuric acid by solvent extraction and stripping. J. Hazard. Mater. 304, 1–9. https://doi.org/10.1016/j.jhazmat.2015.10.049.

Wijdeveld, W.K., Prot, T., Sudintas, G., Kuntke, P., Korving, L., van Loosdrecht, M.C.M., 2022. Pilot-scale magnetic recovery of vivianite from digested sewage sludge. Water Res. 212, 118131 https://doi.org/10.1016/j.watres.2022.118131.

Wilfert, P., Kumar, P.S., Korving, L., Witkamp, G.J., Van Loosdrecht, M.C.M., 2015. The relevance of phosphorus and iron chemistry to the recovery of phosphorus from wastewater: a review. Environ. Sci. Technol. 49, 9400–9414. https://doi.org/10.1021/acs.est.5b00150.

Xu, H., He, P., Gu, W., Wang, G., Shao, L., 2012. Recovery of phosphorus as struvite from sewage sludge ash. J. Environ. Sci. (China) 24, 1533–1538. https://doi.org/10.1016/S1001-0742(11)60969-8.

Yi, X., Huo, G., Tang, W., 2020. Removal of Fe(III) from Ni-Co-Fe chloride solutions using solvent extraction with TBP. Hydrometallurgy 192, 105265. https://doi.org/10.1016/j.hydromet.2020.105265.

Yu, X., Nakamura, Y., Otsuka, M., Omori, D., Haruta, S., 2021. Development of a novel phosphorus recovery system using incinerated sewage sludge ash (ISSA) and phosphorus-selective adsorbent. Waste Manag. 120, 41–49. https://doi.org/10.1016/j.wasman.2020.11.017.

Zhang, G., Chen, D., Wei, G., Zhao, H., Wang, L., Qi, T., Meng, F., Meng, L., 2015. Extraction of iron (III) from chloride leaching liquor with high acidity using tri-n-butyl phosphate and synergistic extraction combined with methyl isobutyl ketone. Sep. Purif. Technol. 150, 132–138. https://doi.org/10.1016/j.seppur.2015.07.001.

Zhang, S., Chen, Y., Zhang, T., Lv, L., Zheng, D., Zhong, B., Tang, S., 2020. Separation of H3PO4 from HCl-wet-processing phosphate rocks leach liquor by TBP: extraction equilibria and mechanism study. Sep. Purif. Technol. 249, 117156 https://doi.org/10.1016/j.seppur.2020.117156.

Zhang, Y., Van der Bruggen, B., Pinoy, L., Meesschaert, B., 2009. Separation of nutrient ions and organic compounds from salts in RO concentrates by standard and monovalent selective ion-exchange membranes used in electrodialysis. J. Memb. Sci. 332, 104–112. https://doi.org/10.1016/j.memsci.2009.01.030.

Zhao, C., Yan, Y., Hou, D., Luan, Z., Jia, Z., 2012. Preparation of high concentration polyaluminum chloride by chemical synthesis-membrane distillation method with self-made hollow fiber membrane. J. Environ. Sci. 24, 834–839. https://doi.org/10.1016/S1001-0742(11)60838-3.

Zhao, H.Z., Liu, C., Xu, Y., Ni, J.R., 2009. High-concentration polyaluminum chloride: preparation and effects of the Al concentration on the distribution and transformation of Al species. Chem. Eng. J. 155, 528–533. https://doi.org/10.1016/j.cej.2009.08.007.